Effective Dirac Hamiltonian for anisotropic honeycomb lattices: Optical properties

M. Oliva-Leyva[1,*] and Gerardo G. Naumis[1,2,†]

[1]*Departamento de Física-Química, Instituto de Física, Universidad Nacional Autónoma de México (UNAM), Apartado Postal 20-364, 01000 México, Distrito Federal, México*

[2]*School of Physics Astronomy and Computational Sciences, George Mason University, Fairfax, Virginia 22030, USA*

(Received 20 November 2015; revised manuscript received 21 December 2015; published 22 January 2016)

We derive the low-energy Hamiltonian for a honeycomb lattice with anisotropy in the hopping parameters. Taking the reported Dirac Hamiltonian for the anisotropic honeycomb lattice, we obtain its optical conductivity tensor and its transmittance for normal incidence of linearly polarized light. Also, we characterize its dichroic character due to the anisotropic optical absorption. As an application of our general findings, which reproduce the previous case of uniformly strained graphene, we study the optical properties of graphene under a nonmechanical distortion.

DOI: 10.1103/PhysRevB.93.035439

I. INTRODUCTION

Among the most unusual properties of graphene, one can cite the linear dispersion relation for electrons and holes at the so-called Dirac points [1]. Therefore, at low energies, electrons and holes behave as two-dimensional massless Dirac fermions, which also present chiral symmetry. This special property provides for the possibility of observing phenomena such as Klein tunneling [2,3], originally predicted for relativistic particle physics [4]. From a practical viewpoint, considering the use of graphene for electronic applications, the unity probability of tunneling through such a barrier, at least for the normal incidence, has resulted in a challenge.

Given the unique mechanical properties of graphene, in particular its striking interval of elastic response [5,6], strain engineering has been an alternative to explore the strain-induced modifications of the electronic properties of graphene [7–10]. Although a theoretical prediction has been made of a strain-induced band-gap opening [11–14], the most interesting strain-induced effect is the experimental observation of Landau-level signatures to zero magnetic field [15,16]. As predicted earlier for carbon nanotubes [17] and subsequently extended to graphene [18–20], the lattice deformation fields can be interpreted in the form of pseudomagnetic fields. Manifestations of such strain-induced pseudomagnetic fields are continuously examined [21–29], even in other materials such as transition-metal dichalcogenides [30] and Weyl semimetals [31].

In the optical context, strain-induced effects in graphene are significant and open an avenue to potential applications [32–34]. The optical properties of graphene are ultimately determined by its electronic structure, which is modified by strain. Needless to say, strain produces anisotropy in the electronic dynamics [35], which is traduced in an anisotropic optical conductivity [36–38] and, finally, in a modulation of the transmittance as a function of the polarization direction [39]. Such modulation of the transmittance has been observed in graphene samples under uniaxial strain [40]. Recently, a theoretical characterization of the transmittance and dichroism was given for graphene under an arbitrary uniform strain, e.g., uniaxial, biaxial, and so forth [41].

Nowadays, synthetic systems with honeycomb lattices are artificially created to mimic the behavior of Dirac quasiparticles [42–44]. The main advantage of these artificial systems is that one can tune, in a controlled and independent manner, the hopping of particles between different lattice sites. As a consequence, in such artificial graphene, one can observe effects which are induced by the anisotropy of the hopping parameters, which are not observable in normal graphene under strain. For example, in normal graphene under a uniaxial strain, it has been predicted that the Dirac cones can merge [11,45]. However, such theoretical prediction requires unrealistically large values of strain. However, in artificial graphene of a different nature, e.g., of cold atoms or photonic crystals, the merging of the Dirac point has been experimentally observed [46]. More recently, in electronic artificial graphene created in a two-dimensional electron gas in a semiconductor heterostructure, the merging of the Dirac point has been demonstrated for realistic experimental conditions [47].

Undoubtedly, artificial graphene paves new opportunities for studying the physics of Dirac quasiparticles in condensed matter. Now, given the excellent possibility to tune the lattice parameters, it seems necessary to have on hand an effective Dirac Hamiltonian, which appropriately describes the dynamics of the quasiparticles in anisotropic configurations of the hopping parameters. In the case of normal graphene under a uniform strain, in the literature one finds various different effective Dirac Hamiltonians. For example, Goerbig *et al.* [48] obtained the effective Dirac Hamiltonian of graphene under a uniaxial strain along the armchair direction. For this problem [48], Harrison's law (quadratic delay) was resorted to evaluate the nearest-neighbor hopping variations induced by deformation. On the other hand, to derive the effective Dirac Hamiltonian of graphene under a uniaxial strain, Pereira *et al.* [39] used a exponential decay to model the nearest-neighbor hopping changes as a function of the strain magnitude. Subsequently, for graphene under a uniform strain, Oliva-Leyva *et al.* [35] derived an effective Dirac Hamiltonian which generalized the reported one in Ref. [39]. However, these reported effective Dirac Hamiltonians do not describe the more general case of a honeycomb lattice with weak

*moliva@fisica.unam.mx
†naumis@fisica.unam.mx

but arbitrary anisotropy of the hopping parameters. Previous Hamiltonians are based on particular laws of the hopping parameters' variations. One of the main objectives of this paper is to give a low-energy Hamiltonian for an anisotropic honeycomb lattice (artificial graphene), able to reproduce the more general conditions of the nearest-neighbor hoppings' variations.

This paper is organized as follows. In Sec. II, we derive the effective Dirac Hamiltonian for a honeycomb lattice with weak anisotropy in the hopping parameters. For this purpose, we start from a nearest-neighbor tight-binding model and carry out an expansion around the real Dirac point. We show how the obtained low-energy Hamiltonian generalizes our previous effective Dirac Hamiltonian of graphene under a uniform strain [35]. Section III is devoted to discuss the optical properties of anisotropic honeycomb lattices, which are assumed by having a linear response to an external oscillating field. Here we give general expressions for the dichroism and transmittance as functions of the variation of hopping parameters. In Sec. IV, our findings are particularized to the case of graphene under a nonmechanical deformation, which cannot represented by means of the strain tensor. Finally, in Sec. V, our conclusions are given.

II. GENERALIZED HONEYCOMB LATTICE

We are interested in the low-energy Hamiltonian, i.e., the effective Dirac Hamiltonian, of a honeycomb lattice with anisotropy in the nearest-neighbor hopping parameters. As unstrained graphene, our lattice consists of a triangular Bravais lattice with a pair of carbon atoms [open and filled circles in Fig. 1(a)] located in its primitive cell. However, we consider that the hoppings between nearest sites are dependent on the direction and, in general, are characterized by three hopping parameters t_1, t_2, and t_3 [see Fig. 1(a)]. Within this nearest-neighbor tight-binding model, one can demonstrate that the Hamiltonian in momentum space can be represented by a (2×2) matrix of the form [49]

$$H = -\sum_{n=1}^{3} t_n \begin{pmatrix} 0 & e^{-i\boldsymbol{k}\cdot\boldsymbol{\delta}_n} \\ e^{i\boldsymbol{k}\cdot\boldsymbol{\delta}_n} & 0 \end{pmatrix}, \tag{1}$$

where $\boldsymbol{\delta}_1, \boldsymbol{\delta}_2, \boldsymbol{\delta}_3$ are the nearest-neighbor vectors. Hereafter, we define the the nearest-neighbor vectors as

$$\boldsymbol{\delta}_1 = \frac{a}{2}(\sqrt{3},1), \quad \boldsymbol{\delta}_2 = \frac{a}{2}(-\sqrt{3},1), \quad \boldsymbol{\delta}_3 = a(0,-1), \tag{2}$$

i.e., we choose the coordinate system xy in a way that the x axis is along the zigzag direction of the honeycomb lattice [see Fig. 1(a)]. We denote the system xy as the crystalline coordinate system.

From Eq. (1) follows that the dispersion relation is given by two bands,

$$E(\boldsymbol{k}) = \pm|t_1 e^{i\boldsymbol{k}\cdot\boldsymbol{\delta}_1} + t_2 e^{i\boldsymbol{k}\cdot\boldsymbol{\delta}_2} + t_3 e^{i\boldsymbol{k}\cdot\boldsymbol{\delta}_3}|. \tag{3}$$

As is well documented, for the isotropic case $t_{1,2,3} = t_0$, the Dirac points $\boldsymbol{K}_D$, which are determined by condition $E(\boldsymbol{K}_D) = 0$, coincide with the corners of the first Brillouin zone. Then, to obtain the Dirac Hamiltonian in this case, one can simply expand the Hamiltonian (1) around a corner, e.g., $\boldsymbol{K}_0 = (\frac{4\pi}{3\sqrt{3}a}, 0)$. However, for the considered anisotropic case, the Dirac points do not coincide with the corners of the first Brillouin zone [as illustrated in Figs. 1(b) and 1(c)] [11,12]. Consequently, to derive the Dirac Hamiltonian, one can no longer expand the Hamiltonian (1) around $\boldsymbol{K}_0$. As recently demonstrated, such expansion around $\boldsymbol{K}_0$ yields an inappropriate Hamiltonian [50]. The appropriate procedure is to *find the position of the Dirac points and carry out the expansion around them* [50–52]. Note that when the hopping anisotropy increases, a gap can appear while the Dirac points disappear. Such effects are characterized by the Hasegawa triangular inequalities [53].

Effective Dirac Hamiltonian

Now let us study the effect of a weak anisotropy given by a small perturbation of the hopping parameters. The perturbed hoppings are given by

$$t_n = t_0(1 + \Delta_n), \tag{4}$$

on the low-energy description. As expressed above, to derive the proper effective Dirac Hamiltonian, it is essential to find the position of the Dirac points [50]. In Appendix A, we show that from the condition $E(\boldsymbol{K}_D) = 0$, up to first order in the

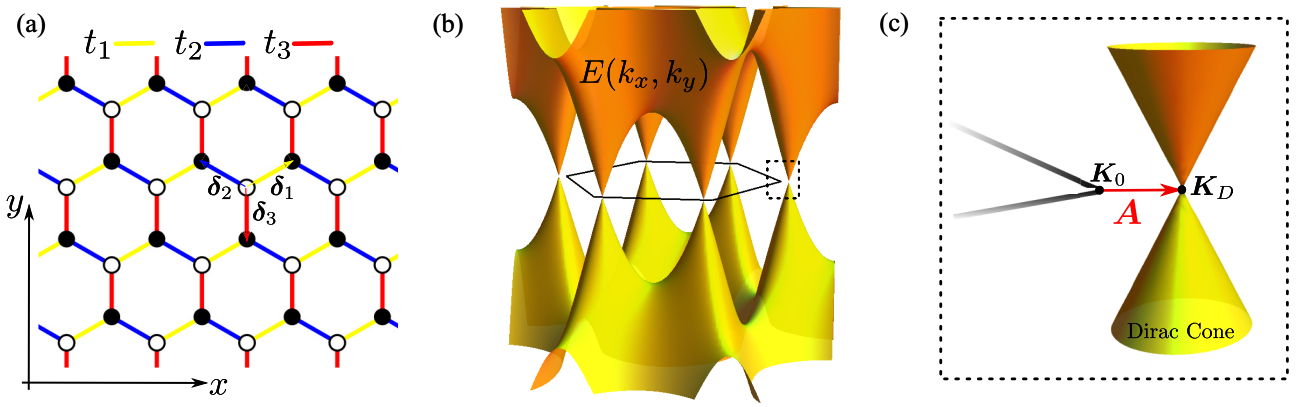

FIG. 1. (a) Honeycomb lattice and hoppings. The primitive cell, in light purple, contains a pair of carbon atoms. (b) Dispersion relation $E(\boldsymbol{k})$ of the anisotropic honeycomb lattice and its hexagonal first Brillouin zone. (c) A zoom of the Dirac cone region shows that the Dirac point $\boldsymbol{K}_D$ is not located at the corner $\boldsymbol{K}_0$ of the hexagonal Brillouin zone. The anisotropy-induced Dirac point shift is given by the vector $\boldsymbol{A}$.

parameters $\{\Delta_n\}$, one can obtain that $\boldsymbol{K}_D$ is given by

$$\boldsymbol{K}_D \approx \boldsymbol{K}_0 + \boldsymbol{A}, \tag{5}$$

where

$$A_x = \frac{1}{3a}(2\Delta_3 - \Delta_1 - \Delta_2), \quad A_y = \frac{1}{\sqrt{3}a}(\Delta_1 - \Delta_2), \tag{6}$$

and $\boldsymbol{K}_0$ presents valley index $\xi = +1$. As is well known [54,55], the shift $\boldsymbol{A}$ of the Dirac point plays the role of an emergent gauge field, similar to a vector potential, when the hopping parameters are position dependent throughout the sample. Thus gauge fields couple with opposite signs to valleys with different index [54,55].

Once the position of $\boldsymbol{K}_D$ is found, we expand the Hamiltonian (1) around the Dirac point by means of $\boldsymbol{k} = \boldsymbol{K}_D + \boldsymbol{q}$. Following this approach up to first order in the parameters $\{\Delta_n\}$, which is the leading order used throughout the rest of the paper, we derive that the effective Dirac Hamiltonian results in (see Appendix B)

$$H = \hbar v_F \boldsymbol{\sigma} \cdot (\bar{\boldsymbol{I}} + \bar{\boldsymbol{\Delta}}) \cdot \boldsymbol{q}, \tag{7}$$

where $v_F = 3t_0 a/2\hbar$ is the Fermi velocity for the unperturbed honeycomb lattice, $\boldsymbol{\sigma} = (\sigma_x, \sigma_y)$ are the nondiagonal Pauli matrices, $\bar{\boldsymbol{I}}$ is the 2×2 identity matrix, and $\bar{\boldsymbol{\Delta}}$ is the symmetric matrix

$$\bar{\boldsymbol{\Delta}} = \begin{pmatrix} \frac{1}{3}(2\Delta_1 + 2\Delta_2 - \Delta_3) & \frac{1}{\sqrt{3}}(\Delta_1 - \Delta_2) \\ \frac{1}{\sqrt{3}}(\Delta_1 - \Delta_2) & \Delta_3 \end{pmatrix}. \tag{8}$$

Let us note some important remarks about our generalized Hamiltonian (7). First of all, when the three hopping parameters $\{t_n\}$ are equal to $t_0(1 + \Delta)$, we have that $\bar{\boldsymbol{\Delta}} = \Delta \bar{\boldsymbol{I}}$. Then, Eq. (7) reproduces the expected result $\hbar v_F(1 + \Delta)\boldsymbol{\sigma} \cdot \boldsymbol{q}$, which is just a renormalization of the Fermi velocity. In general, from Eq. (7), one can recognize a generalized Fermi velocity tensor as

$$\bar{\boldsymbol{v}} = v_F(\bar{\boldsymbol{I}} + \bar{\boldsymbol{\Delta}}), \tag{9}$$

whose matrix character is due to the shape of the isoenergetic contours around $\boldsymbol{K}_D$, which are rotated ellipses. Only for the case that $t_1 = t_2$ ($\Delta_1 = \Delta_2$), the Fermi velocity tensor is diagonal with respect to the chosen crystalline coordinate system xy. In this case, the principal axes of the isoenergetic ellipses are collinear with the xy axes.

The general character of Eq. (7) enables one to obtain the effective Dirac Hamiltonian for any form of variation of the hopping parameters. For example, in Ref. [35], for the case of graphene under a spatially uniform strain, the authors assumed that to first order in the strain tensor $\bar{\boldsymbol{\epsilon}}$, the hopping parameters are approximated by $t_n \approx t_0(1 - \beta \boldsymbol{\delta}_n \cdot \bar{\boldsymbol{\epsilon}} \cdot \boldsymbol{\delta}_n / a^2)$, where β is the electron Grüneisen parameter. Thus, in this particular case, $\Delta_n = -\beta \boldsymbol{\delta}_n \cdot \bar{\boldsymbol{\epsilon}} \cdot \boldsymbol{\delta}_n / a^2$ and, then, from Eq. (8), one obtain that $\bar{\boldsymbol{\Delta}} = -\beta \bar{\boldsymbol{\epsilon}}$, as reported in Ref. [35]. Similarly, our generalized expressions (7) and (8) can be used to reproduce the effective Hamiltonian reported in Ref. [48], where a different form of variation of the hopping parameters (Harrison's law) was assumed.

It is important to emphasize that the expression (8) for the matrix $\bar{\boldsymbol{\Delta}}$ is referred to the crystalline coordinate system xy. In general, if one chooses an arbitrary coordinate system $x'y'$, rotated at an angle ϕ with respect to the system xy, then the new components of $\bar{\boldsymbol{\Delta}}$ can be found by means of the transformation rules of a second-order Cartesian tensor. In other words, $\bar{\boldsymbol{\Delta}}$ is a second-order Cartesian tensor, whose explicit form (8) is given with respect to the crystalline coordinate system xy.

III. OPTICAL CONDUCTIVITY

Let us now study the optical properties of those anisotropic electronic honeycomb fermionic lattices that exhibit a linear response to an external electric field of frequency w. For this purpose, we first obtain the optical conductivity tensor $\bar{\sigma}_{ij}(w)$ by combining the Hamiltonian (7) and the Kubo formula. Following the representation used in Refs. [56,57], the optical conductivity $\sigma_{ij}(w)$ can be written as a double integral with respect to two energies E, E':

$$\bar{\sigma}_{ij}(w) = \frac{i}{\hbar} \iint \mathrm{Tr}\{j_i \delta(H - E') j_j \delta(H - E)\} \times \frac{1}{E - E' + w - i\alpha} \frac{f(E) - f(E')}{E - E'} dE dE', \tag{10}$$

where $f(E) = \{1 + \exp[E/(k_B T)]\}^{-1}$ is the Fermi function at temperature T and $j_l = -ie[H, r_l]$ is the current operator in the l direction, with $l = x, y$.

To calculate the integral (10), it is convenient to carry out the change of variables,

$$\boldsymbol{q} = (\bar{\boldsymbol{I}} + \bar{\boldsymbol{\Delta}})^{-1} \cdot \boldsymbol{q}^*. \tag{11}$$

In the new variables (q_x^*, q_y^*), the Hamiltonian (7) becomes $H = \hbar v_F \boldsymbol{\sigma} \cdot \boldsymbol{q}^*$, corresponding to an unperturbed honeycomb lattice, as unstrained graphene. On the other hand, the current operator components transform as

$$\begin{aligned} j_x &= -ie[H, r_x] = e\frac{\partial H}{\partial q_x} \\ &= e\left(\frac{\partial H}{\partial q_x^*}\frac{\partial q_x^*}{\partial q_x} + \frac{\partial H}{\partial q_y^*}\frac{\partial q_y^*}{\partial q_x}\right) \\ &= (1 + \bar{\Delta}_{xx}) j_x^* + \bar{\Delta}_{xy} j_y^*, \end{aligned} \tag{12}$$

and, analogously,

$$j_y = (1 + \bar{\Delta}_{yy}) j_y^* + \bar{\Delta}_{xy} j_x^*, \tag{13}$$

where $j_x^* = e(\partial H/\partial q_x^*)$ and $j_y^* = e(\partial H/\partial q_y^*)$ are the current operator components for the case of the unperturbed honeycomb lattice.

Then, substituting Eqs. (12) and (13) into Eq. (10), we obtain

$$\bar{\sigma}_{xx}(w) \simeq (1 + 2\bar{\Delta}_{xx}) J \sigma_0(w), \tag{14}$$

$$\bar{\sigma}_{yy}(w) \simeq (1 + 2\bar{\Delta}_{yy}) J \sigma_0(w), \tag{15}$$

$$\bar{\sigma}_{xy}(w) = \bar{\sigma}_{yx}(w) \simeq 2\bar{\Delta}_{xy} J \sigma_0(w), \tag{16}$$

where J is the Jacobian determinant of the transformation (11) and $\sigma_0(w)$ is the optical conductivity of the unperturbed honeycomb lattice. Note that as an explicit expression for $\sigma_0(w)$, one can use the reported optical conductivity of unstrained graphene [57–59].

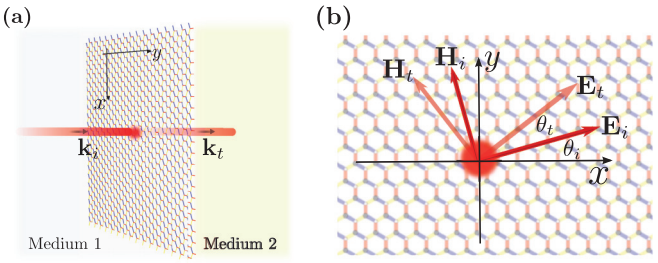

FIG. 2. (a) Scattering problem for normal incidence between two media with the anisotropic honeycomb lattice separating them. The z direction is chosen along the propagation of the electromagnetic wave. $\boldsymbol{k}_i$ and $\boldsymbol{k}_t$ represent the wave vectors of the incident and transmitted waves, respectively. (b) Schematic representation of the dichroism induced by the anisotropic absorption of the honeycomb lattice. The electromagnetic fields lie in the lattice plane.

Finally, from Eqs. (14)–(16), it follows that the optical conductivity tensor for the anisotropic honeycomb lattice results in

$$\bar{\boldsymbol{\sigma}}(w) \simeq \sigma_0(w)[\bar{\boldsymbol{I}} + 2\bar{\boldsymbol{\Delta}} - \mathrm{Tr}(\bar{\boldsymbol{\Delta}})\bar{\boldsymbol{I}}]. \tag{17}$$

In other words, a Dirac system described by the generalized Hamiltonian (7) presents an anisotropic optical response given by Eq. (17), independently of the expression of matrix $\bar{\boldsymbol{\Delta}}$. Now substituting Eq. (8) into Eq. (17), we obtain the explicit form of the optical conductivity tensor for the anisotropic honeycomb lattice, with respect to the crystalline coordinate system xy.

Dichroism and transmittance

The anisotropy of the optical absorption yields two effects: dichroism and modulation of the transmittance as a function of the polarization direction. To examine such effects, let us consider normal incidence of linearly polarized light between two dielectric media separated by our anisotropic honeycomb lattice, as illustrated in Fig. 2(a). From the boundary conditions for the electromagnetic field on the interface between both media, one can obtain that the electric fields of the incident and transmitted waves, $\boldsymbol{E}_i$ and $\boldsymbol{E}_t$, respectively, are related by [41]

$$\boldsymbol{E}_i = \frac{1}{2}\sqrt{\frac{\mu_1}{\epsilon_1}}\left[\left(\sqrt{\frac{\epsilon_1}{\mu_1}} + \sqrt{\frac{\epsilon_2}{\mu_2}}\right)\bar{\boldsymbol{I}} + \bar{\boldsymbol{\sigma}}\right]\cdot \boldsymbol{E}_t, \tag{18}$$

where $\epsilon_{1,2}$ are the electrical permittivities and $\mu_{1,2}$ are the magnetic permeabilities. Note that, in general, the anisotropy of the conductivity $\bar{\boldsymbol{\sigma}}$ produces that $\boldsymbol{E}_i$ and $\boldsymbol{E}_t$ are not collinear [see Fig. 2(b)]. Analogously, the magnetic fields, $\boldsymbol{H}_i$ and $\boldsymbol{H}_t$, fulfill the same relation.

Now, from Eq. (18), the calculation of the transmittance is straightforward [41]:

$$T(\theta_i) = \frac{|\boldsymbol{E}_t \times \boldsymbol{H}_t|}{|\boldsymbol{E}_i \times \boldsymbol{H}_i|} = \frac{\sqrt{\epsilon_2/\mu_2}|\boldsymbol{E}_t|^2}{\sqrt{\epsilon_1/\mu_1}|\boldsymbol{E}_i|^2},$$
$$\approx T_0\left(1 - \frac{2\sqrt{\mu_1\mu_2}}{\sqrt{\epsilon_1\mu_2} + \sqrt{\epsilon_2\mu_1}}\boldsymbol{e}_i^{\mathsf{T}}\cdot \mathrm{Re}\bar{\boldsymbol{\sigma}}\cdot \boldsymbol{e}_i\right), \tag{19}$$

where T_0 is the transmittance for normal incidence between two media in the absence of the anisotropic honeycomb lattice as interface and $\boldsymbol{e}_i^{\mathsf{T}} = (\cos\theta_i, \sin\theta_i)$, with θ_i being the incident polarization angle θ_i.

To illustrate even more clearly the dichroism and the modulation of $T(\theta_i)$ induced by the anisotropic honeycomb lattice, it is convenient to consider that the chemical potential equals zero for the lattice. In consequence, for the domain of infrared and visible frequencies, in Eq. (17) $\sigma_0(w)$ can be replaced by the universal and frequency-independent value $e^2/(4\hbar)$ [59,60]. Additionally, if both media are vacuum, then from Eqs.(17)–(19) we obtain

$$\theta_t - \theta_i \approx \frac{\pi\alpha}{2}A\sin(2\theta_i - \theta_0) \ \text{(in radians)}, \tag{20}$$

$$T(\theta_i) \approx 1 - \pi\alpha[1 + A\cos(2\theta_i - \theta_0)], \tag{21}$$

where

$$A = \sqrt{(\bar{\Delta}_{xx} - \bar{\Delta}_{yy})^2 + 4\bar{\Delta}_{xy}^2} = \sqrt{(\mathrm{Tr}\bar{\boldsymbol{\Delta}})^2 - 4\mathrm{Det}\bar{\boldsymbol{\Delta}}}, \tag{22}$$

$\sin\theta_0 = 2\bar{\Delta}_{xy}/A$ [$\cos\theta_0 = (\bar{\Delta}_{xx} - \bar{\Delta}_{yy})/A$], and α is the fine-structure constant.

It can be immediately verified that for $\bar{\boldsymbol{\Delta}} = 0$, the dichroism disappears and $T(\theta_i)$ reduces to $1 - \pi\alpha$ ($\approx$97.7%), which is the transmittance of unstrained graphene [60]. Expressions (20) and (21) clearly show π-periodic modulations of the dichroism and transmittance with respect to the incident polarization angle θ_i, which is due to the physical equivalence between θ_i and $\theta_i + \pi$, for normal incidence of linearly polarized light. From Eq. (20) follows that the principal directions of $\bar{\boldsymbol{\Delta}}$ can be determined by monitoring the polarization angles θ_i for which the incident and transmitted polarizations coincide. At the same time, Eq. (21) shows that the principal directions of $\bar{\boldsymbol{\Delta}}$ can be determined by measuring the polarization angles θ_i for which the transmittance takes its minimum or maximum values. Also, it is important to note that while the phase θ_0 of both modulations is dependent on the coordinate system orientation, the amplitude A is independent of any orientation of the coordinate system, as physically expected, because A is given as a function of the invariants $\mathrm{Tr}\bar{\boldsymbol{\Delta}}$ and $\mathrm{Det}\bar{\boldsymbol{\Delta}}$.

So far, our discussion of dichroism and transmittance is general for an anisotropic Dirac system described by Eq. (7). By substituting Eq. (8) into Eqs. (20) and (21), one obtains the explicit form of such effects for the anisotropic honeycomb lattice with respect to the crystalline coordinate system xy.

IV. APPLICATION

As an application of the obtained results, we consider a deformation of graphene lattice, as illustrated in Fig. 3. Here the primitive vectors $\boldsymbol{a}_1$ and $\boldsymbol{a}_2$ remain undeformed, while the atom of basis, denoted by an open circle, is displaced as a vector $\boldsymbol{u}$ in an arbitrary direction. This deformation of the graphene lattice is basically a displacement, given by $\boldsymbol{u}$, of the open-circles sublattice with respect to the filled-circles sublattice. A possible scenario for such deformation could occur in graphene grown on a substrate with an appropriate combination of lattice mismatch between the two crystals [40,61].

It is important to emphasize that the considered nonmechanical deformation cannot be represented by means of the standard strain tensor. Therefore, the previous reported results

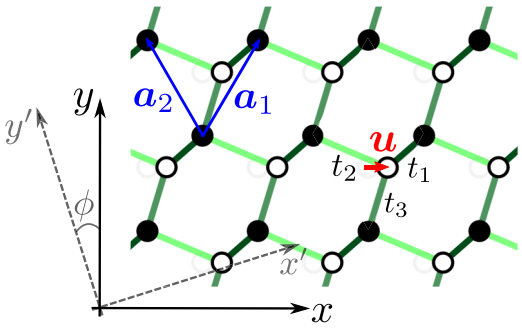

FIG. 3. Scheme of the modified graphene lattice. The red arrow represents the displacement $\boldsymbol{u}$ of the open-circles sublattice.

for graphene under a uniform strain, e.g., the effective Dirac Hamiltonian reported in [35] and its optical properties [37,41] cannot be used to characterize such deformation. This fact clearly shows the relevance and usefulness of the general treatment developed in the present work.

The new nearest-neighbor vectors $\boldsymbol{\delta}'_n$ are related to the unstrained nearest-neighbor vectors $\boldsymbol{\delta}_n$ by means of $\boldsymbol{\delta}'_n = \boldsymbol{\delta}_n - \boldsymbol{u}$. However, the reciprocal lattice of our modified graphene lattice remains undeformed because the direct lattice, determined by $\boldsymbol{a}_1$ and $\boldsymbol{a}_2$, is undistorted. The last is a notable difference with respect to the case of strained graphene by means of mechanical stress, for which the lattice vectors are deformed.

As in Sec. II, if we begin from a nearest-neighbor approach, it is easy to demonstrate that the dispersion relation for this modified graphene lattice reads

$$\begin{aligned} E(\boldsymbol{k}) &= \pm|t_1 e^{i\boldsymbol{k}\cdot(\boldsymbol{\delta}_1-\boldsymbol{u})} + t_2 e^{i\boldsymbol{k}\cdot(\boldsymbol{\delta}_2-\boldsymbol{u})} + t_3 e^{i\boldsymbol{k}\cdot(\boldsymbol{\delta}_3-\boldsymbol{u})}| \\ &= \pm|t_1 e^{i\boldsymbol{k}\cdot\boldsymbol{\delta}_1} + t_2 e^{i\boldsymbol{k}\cdot\boldsymbol{\delta}_2} + t_3 e^{i\boldsymbol{k}\cdot\boldsymbol{\delta}_3}|, \end{aligned} \tag{23}$$

where we characterize the variation of the hopping parameters in the usual form: $t_n = t_0 \exp[-\beta(|\boldsymbol{\delta}'_n|/a - 1)]$ [11]. Note that Eq. (23) coincides with Eq. (3), so the modified graphene lattice can be considered as a particular case of the generalized honeycomb lattice examined in Sec. II. Therefore, now we can particularize all general previous results for the modified graphene lattice.

Effective Dirac Hamiltonian. Writing the variation of the hopping parameters to first order in $\boldsymbol{u}$, one gets

$$\begin{aligned} t_n &= t_0 \exp[-\beta(|\boldsymbol{\delta}_n - \boldsymbol{u}|/a - 1)] \\ &\approx t_0(1 + \beta\boldsymbol{\delta}_n \cdot \boldsymbol{u}/a^2), \end{aligned} \tag{24}$$

and thus, for this case, one can identify from Eq. (4) that $\Delta_n = \beta\boldsymbol{\delta}_n \cdot \boldsymbol{u}/a^2$. Consequently, from Eqs. (7) and (8), the effective Dirac Hamiltonian of the modified graphene lattice results in

$$H = \hbar v_F \boldsymbol{\sigma} \cdot (\bar{\boldsymbol{I}} + \bar{\boldsymbol{\Delta}}^u) \cdot \boldsymbol{q}, \tag{25}$$

where the matrix $\bar{\boldsymbol{\Delta}}^u$ depends on the components of the vector $\boldsymbol{u}$ as

$$\bar{\boldsymbol{\Delta}}^u = \frac{\beta}{a}\begin{pmatrix} u_y & u_x \\ u_x & -u_y \end{pmatrix}. \tag{26}$$

It can be immediately verified that for $\boldsymbol{u} = 0$, one recovers the case of unstrained graphene. Note that $\mathrm{Tr}\bar{\boldsymbol{\Delta}}^u = 0$, which is because the studied deformation does not vary the area of the graphene sample. This fact is analogous to having a pure shear strain.

The form (26) of the tensor $\bar{\boldsymbol{\Delta}}^u$ is referred to as the crystalline coordinate system xy. Now let us give its general expression with respect to an arbitrary coordinate system $x'y'$, which is inclined to xy at an angle ϕ. Using the transformation rules of a second-order Cartesian tensor, we find

$$\bar{\Delta}^u_{x'x'} = -\bar{\Delta}^u_{y'y'} = \frac{\beta}{a}(u_{y'}\cos 3\phi + u_{x'}\sin 3\phi), \tag{27}$$

$$\bar{\Delta}^u_{x'y'} = \bar{\Delta}^u_{y'x'} = \frac{\beta}{a}(-u_{y'}\sin 3\phi + u_{x'}\cos 3\phi), \tag{28}$$

where $u_{x'}$ and $u_{y'}$ are the components of the vector $\boldsymbol{u}$ with respect to the system $x'y'$. These expressions for the tensor $\bar{\boldsymbol{\Delta}}^u(\phi)$ exhibit a clear periodicity of $2\pi/3$ in ϕ, which reflects the trigonal symmetry of the underlying honeycomb lattice.

Optical properties. From Eqs. (17) and (26), the optical conductivity for the modified graphene lattice immediately follows as

$$\begin{aligned} \bar{\boldsymbol{\sigma}}^u(w) &= \sigma_0(w)(\bar{\boldsymbol{I}} + 2\bar{\boldsymbol{\Delta}}^u) \\ &= \sigma_0(w)\begin{pmatrix} 1 + 2\beta u_y/a & 2\beta u_x/a \\ 2\beta u_x/a & 1 - 2\beta u_y/a \end{pmatrix}, \end{aligned} \tag{29}$$

with respect to the crystalline coordinate system xy. At the same time, from Eqs. (20) and (21), one obtains that for normal incidence of linearly polarized light, the dichroism and the transmittance are characterized by

$$\theta_t - \theta_i \approx \frac{\pi\alpha\beta}{a}(u_y \sin 2\theta_i - u_x \cos 2\theta_i), \tag{30}$$

$$T(\theta_i) \approx 1 - \pi\alpha - \frac{2\pi\alpha\beta}{a}(u_y \cos 2\theta_i + u_x \sin 2\theta_i), \tag{31}$$

where the incident polarization angle θ_i is measured with respect to the x axis of the crystalline coordinate system.

In Fig. 4, we display the evaluated expressions (30) and (31) for two different displacements, $\boldsymbol{u}_1/a = (0.05,0)$ and $\boldsymbol{u}_2/a = (0.04,0.03)$. Such deformations present the same modulation amplitude either for the rotation of the transmitted field (dichroism) or for the transmittance. The reason is simple. From (31), it follows that the transmittance modulation amplitude $\triangle T$ is determined by the module of the vector $\boldsymbol{u}$: $\triangle T = 2\pi\alpha\beta|\boldsymbol{u}|/a$. Note that $|\boldsymbol{u}_1| = |\boldsymbol{u}_2|$, and therefore, $\triangle T_1 = \triangle T_2$. The analogous argument is valid for the modulation amplitude of the rotation of the transmitted field: $\triangle\phi = \pi\alpha\beta|\boldsymbol{u}|/a$.

Nowadays, measurements of transmittance can be used to characterize the deformation state in the graphene sample [40,41].

To complete, let us point out how Eq. (31) serves to characterize the strain state of our modified graphene lattice by means of two measurements of transmittance. Measuring the transmittance at $\theta_i = 0$ and $\theta_i = \pi/4$, from Eq. (31) one obtains

$$u_x = \frac{a}{2\pi\alpha\beta}[1 - \pi\alpha - T(\pi/4)], \tag{32}$$

$$u_y = \frac{a}{2\pi\alpha\beta}[1 - \pi\alpha - T(0)], \tag{33}$$

and, in this manner, the strain state can be determined.

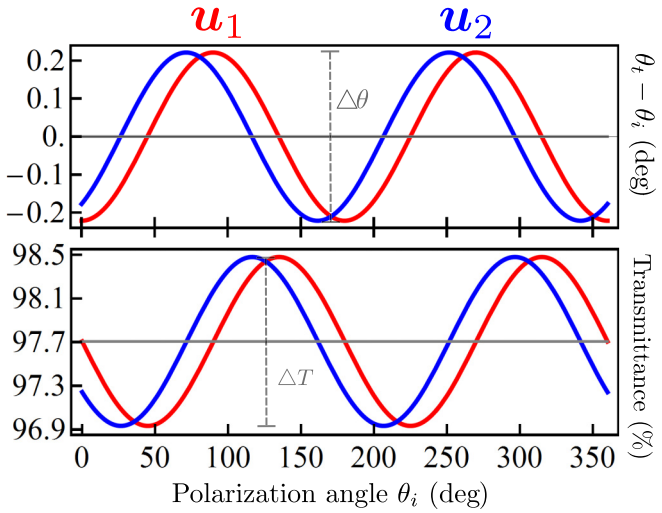

FIG. 4. Rotation of the transmitted field (top panel) and transmittance (bottom panel) as a function of the incident polarization angle for two different deformations. The red curves correspond to the displacement $\boldsymbol{u}_1/a = (0.05,0)$, while the blue curves correspond to the displacement $\boldsymbol{u}_2/a = (0.04,0.03)$.

V. CONCLUSION

In summary, starting from a nearest-neighbor tight-binding model, we derived the effective Dirac Hamiltonian of an anisotropic honeycomb lattice, beyond strained normal graphene. This general Hamiltonian results in a useful tool for studying the anisotropic dynamics of Dirac quasiparticles in artificial graphene. Our generalized Hamiltonian (7) has a remarkable merit with respect to previous effective Dirac Hamiltonians. It is not limited to a particular law of the hopping parameters' variation. Moreover, it is an excellent starting point for obtaining the effective Dirac Hamiltonian in the case of position-dependent anisotropy of the honeycomb lattice [50]. We also obtained the optical conductivity tensor of the anisotropic honeycomb lattice and showed how such anisotropic optical absorption produces a modulation of the transmittance and of the dichroism as a function of the incident polarization angle. Our findings could provide a platform to characterize the anisotropy in electric artificial graphene by means of optical measurements. At the same time, they could be used for tailoring the optical properties of electric artificial graphene.

ACKNOWLEDGMENTS

This work was supported by UNAM-DGAPA-PAPIIT, Project No. IN-102513. M.O.L. acknowledges to CONACYT (Mexico) for a scholarship for doctoral studies. G.G.N. is thankful for the support of a PASPA scholarship for a sabbatical leave at George Mason University.

APPENDIX A

Here we provide the derivation of the expressions (6) for the shift vector $\boldsymbol{A}$ of the Dirac point $\boldsymbol{K}_D$.

The condition $E(\boldsymbol{K}_D) = 0$, which defines the Dirac points $\boldsymbol{K}_D$, can be equivalently rewritten as

$$\sum_{n=1}^{3} t_n e^{i\boldsymbol{K}_D\cdot\boldsymbol{\delta}_n} = 0. \tag{A1}$$

In the isotropic case $t_n = t_0$, the Dirac points coincide with the corners of the first Brillouin zone, in particular $\boldsymbol{K}_D = \boldsymbol{K}_0 = (\frac{4\pi}{3\sqrt{3}a},0)$, with $\boldsymbol{K}_0$ being a corner with valley index $+1$. For the anisotropic case $t_n = t_0(1+\Delta_n)$, the Dirac points do not coincide with the corners of the first Brillouin zone, in particular $\boldsymbol{K}_D \neq \boldsymbol{K}_0$. Then, one can propose the position of $\boldsymbol{K}_D$ in the form

$$\boldsymbol{K}_D = \boldsymbol{K}_0 + \boldsymbol{A} + O\left(\Delta_n^2\right), \tag{A2}$$

where the unknown shift $\boldsymbol{A}$ will be looked for as a lineal combination on the parameters $\{\Delta_n\}$. Now, substituting Eq. (A2) into Eq. (A1) results in

$$\begin{aligned}
&\sum_{n=1}^{3} t_0(1+\Delta_n)e^{i[\boldsymbol{K}_0+\boldsymbol{A}+O(\Delta_n^2)]\cdot\boldsymbol{\delta}_n} = 0,\\
&\sum_{n=1}^{3}\left[1+\Delta_n + i\boldsymbol{A}\cdot\boldsymbol{\delta}_n + O\left(\Delta_n^2\right)\right]e^{i\boldsymbol{K}_0\cdot\boldsymbol{\delta}_n} = 0,\\
&\quad -3aA_x - \Delta_1 - \Delta_2 + 2\Delta 3\\
&\quad + i(-3aA_y + \sqrt{3}\Delta_1 - \sqrt{3}\Delta_2) + O\left(\Delta_n^2\right) = 0.
\end{aligned} \tag{A3}$$

Thus, one obtains that the shift $\boldsymbol{A}$ is given by

$$A_x = \frac{1}{3a}(2\Delta_3 - \Delta_1 - \Delta_2), \quad A_y = \frac{1}{\sqrt{3}a}(\Delta_1 - \Delta_2), \tag{A4}$$

which is our Eq. (6). Following a similar calculation, the Dirac point shift with respect to the corner $\boldsymbol{K}_0^{'} = (-\frac{4\pi}{3\sqrt{3}a},0)$, with valley index -1, results in $-\boldsymbol{A}$.

APPENDIX B

In this section, we present the details of the calculations to derive the effective Hamiltonian around $\boldsymbol{K}_D = \boldsymbol{K}_0 + \boldsymbol{A}$. Also, these calculations can be taken as an alternative proof of Eq. (6), as pointed out below.

Considering momenta close to the Dirac point $\boldsymbol{K}_D$, i.e., $\boldsymbol{k} = \boldsymbol{K}_D + \boldsymbol{q}$, and expanding to first order in $\boldsymbol{q}$ and $\{\Delta_n\}$, Hamiltonian (1) transforms as

$$\begin{aligned}
H &= -\sum_{n=1}^{3} t_n \begin{pmatrix} 0 & e^{-i(\boldsymbol{K}_0+\boldsymbol{A}+\boldsymbol{q})\cdot\boldsymbol{\delta}_n} \\ e^{i(\boldsymbol{K}_0+\boldsymbol{A}+\boldsymbol{q})\cdot\boldsymbol{\delta}_n} & 0 \end{pmatrix}\\
&= -\sum_{n=1}^{3} t_0(1+\Delta_n)\begin{pmatrix} 0 & e^{-i\boldsymbol{K}_0\cdot\boldsymbol{\delta}_n} \\ e^{i\boldsymbol{K}_0\cdot\boldsymbol{\delta}_n} & 0 \end{pmatrix}\\
&\quad\times(\bar{\boldsymbol{I}} + i\sigma_z\boldsymbol{A}\cdot\boldsymbol{\delta}_n)(\bar{\boldsymbol{I}} + i\sigma_z\boldsymbol{q}\cdot\boldsymbol{\delta}_n)\\
&= -t_0\sum_{n=1}^{3}\left(i\frac{\boldsymbol{\sigma}\cdot\boldsymbol{\delta}_n}{a}\sigma_z\right)[\bar{\boldsymbol{I}} + i\sigma_z\boldsymbol{q}\cdot\boldsymbol{\delta}_n + i\sigma_z\boldsymbol{A}\cdot\boldsymbol{\delta}_n\\
&\quad + \Delta_n\bar{\boldsymbol{I}} - (\boldsymbol{q}\cdot\boldsymbol{\delta}_n)(\boldsymbol{A}\cdot\boldsymbol{\delta}_n)\bar{\boldsymbol{I}}],
\end{aligned} \tag{B1}$$

where it has been assumed that the $\boldsymbol{A}$ vector is given by Eq. (6) and $\boldsymbol{K}_0 = (\frac{4\pi}{3\sqrt{3}a}, 0)$ has valley index $\xi = +1$. Collecting the contribution of each term in this expression, one obtains

$$-t_0 \sum_{n=1}^{3} \left(i \frac{\boldsymbol{\sigma} \cdot \boldsymbol{\delta}_n}{a} \sigma_z \right) = 0, \tag{B2}$$

$$-t_0 \sum_{n=1}^{3} \left(i \frac{\boldsymbol{\sigma} \cdot \boldsymbol{\delta}_n}{a} \sigma_z \right) (i \sigma_z \boldsymbol{q} \cdot \boldsymbol{\delta}_n) = \hbar v_F \boldsymbol{\sigma} \cdot \boldsymbol{q}, \tag{B3}$$

$$-t_0 \sum_{n=1}^{3} \left(i \frac{\boldsymbol{\sigma} \cdot \boldsymbol{\delta}_n}{a} \sigma_z \right) (i \sigma_z \boldsymbol{A} \cdot \boldsymbol{\delta}_n) = \hbar v_F \boldsymbol{\sigma} \cdot \boldsymbol{A}, \tag{B4}$$

$$-t_0 \sum_{n=1}^{3} \left(i \frac{\boldsymbol{\sigma} \cdot \boldsymbol{\delta}_n}{a} \sigma_z \right) \Delta_n = -\hbar v_F \boldsymbol{\sigma} \cdot \boldsymbol{A}, \tag{B5}$$

$$t_0 \sum_{n=1}^{3} \left(i \frac{\boldsymbol{\sigma} \cdot \boldsymbol{\delta}_n}{a} \sigma_z \right) (\boldsymbol{q} \cdot \boldsymbol{\delta}_n)(\boldsymbol{A} \cdot \boldsymbol{\delta}_n) = \hbar v_F \boldsymbol{\sigma} \cdot \bar{\boldsymbol{\Delta}} \cdot \boldsymbol{q}, \tag{B6}$$

where the $\bar{\boldsymbol{\Delta}}$ matrix is given by Eq. (8). Then, taking into account the contribution of each term in Eq. (B1), the effective Dirac Hamiltonian around K_D has the form

$$H = \hbar v_F \boldsymbol{\sigma} \cdot (\bar{\boldsymbol{I}} + \bar{\boldsymbol{\Delta}}) \cdot \boldsymbol{q}. \tag{B7}$$

This result also proves that the Dirac point $\boldsymbol{K}_D$ is given by Eqs. (5) and (6). Note that in the Hamiltonian (B7), all terms are $O(\boldsymbol{q})$, which is a consequence of an expansion around the real Dirac point and, therefore, this proves that the expression (6) for the shift $\boldsymbol{A}$ of the Dirac point is correct.

For $\boldsymbol{K}_0$ with valley index $\xi = -1$, the calculation is analogous and the effective Dirac Hamiltonian results,

$$H = \hbar v_F \boldsymbol{\sigma}^* \cdot (\bar{\boldsymbol{I}} + \bar{\boldsymbol{\Delta}}) \cdot \boldsymbol{q}, \tag{B8}$$

where $\boldsymbol{\sigma}^* = (\sigma_x, -\sigma_y)$.

[1] A. H. Castro Neto, F. Guinea, N. M. R. Peres, K. S. Novoselov, and A. K. Geim, Rev. Mod. Phys. **81**, 109 (2009).
[2] M. I. Katsnelson, K. S. Novoselov, and A. K. Geim, Nat. Phys. **2**, 620 (2006).
[3] A. F. Young and P. Kim, Nat. Phys. **5**, 222 (2009).
[4] A. Calogeracos and N. Dombey, Contemp. Phys. **40**, 313 (1999).
[5] C. Lee, X. Wei, J. W. Kysar, and J. Hone, Science **321**, 385 (2008).
[6] A. Castellanos-Gomez, V. Singh, H. S. J. van der Zant, and G. A. Steele, Ann. Phys. **527**, 27 (2015).
[7] V. M. Pereira and A. H. Castro Neto, Phys. Rev. Lett. **103**, 046801 (2009).
[8] F. Guinea, Solid State Commun. **152**, 1437 (2012).
[9] B. Wang, Y. Wang, and Y. Liu, Funct. Mater. Lett. **08**, 1530001 (2015).
[10] B. Amorim, A. Cortijo, F. de Juan, A. G. Grushin, F. Guinea, A. Gutiérrez-Rubio, H. Ochoa, V. Parente, R. Roldán, P. San-José, J. Schiefele, M. Sturla, and M. A. H. Vozmediano, arXiv:1503.00747.
[11] V. M. Pereira, A. H. Castro Neto, and N. M. R. Peres, Phys. Rev. B **80**, 045401 (2009).
[12] Y. Li, X. Jiang, Z. Liu, and Z. Liu, Nano Res. **3**, 545 (2010).
[13] G. Cocco, E. Cadelano, and L. Colombo, Phys. Rev. B **81**, 241412 (2010).
[14] G. Gui, D. Morgan, J. Booske, J. Zhong, and Z. Ma, Appl. Phys. Lett. **106**, 053113 (2015).
[15] N. Levy, S. A. Burke, K. L. Meaker, M. Panlasigui, A. Zettl, F. Guinea, A. H. C. Neto, and M. F. Crommie, Science **329**, 544 (2010).
[16] J. Lu, A. C. Neto, and K. P. Loh, Nat. Commun. **3**, 823 (2012).
[17] H. Suzuura and T. Ando, Phys. Rev. B **65**, 235412 (2002).
[18] A. F. Morpurgo and F. Guinea, Phys. Rev. Lett. **97**, 196804 (2006).
[19] S. V. Morozov, K. S. Novoselov, M. I. Katsnelson, F. Schedin, L. A. Ponomarenko, D. Jiang, and A. K. Geim, Phys. Rev. Lett. **97**, 016801 (2006).
[20] F. Guinea, M. I. Katsnelson, and A. K. Geim, Nat. Phys. **6**, 30 (2010).
[21] J. V. Sloan, Alejandro A. Pacheco Sanjuan, Z. Wang, C. Horvath, and S. Barraza-Lopez, Phys. Rev. B **87**, 155436 (2013).
[22] D. A. Gradinar, M. Mucha-Kruczyński, H. Schomerus, and V. I. Fal'ko, Phys. Rev. Lett. **110**, 266801 (2013).
[23] W.-Y. He and L. He, Phys. Rev. B **88**, 085411 (2013).
[24] R. Carrillo-Bastos, D. Faria, A. Latgé, F. Mireles, and N. Sandler, Phys. Rev. B **90**, 041411 (2014).
[25] Z. Qi, A. L. Kitt, H. S. Park, V. M. Pereira, D. K. Campbell, and A. H. Castro Neto, Phys. Rev. B **90**, 125419 (2014).
[26] R. Burgos, J. Warnes, L. R. F. Lima, and C. Lewenkopf, Phys. Rev. B **91**, 115403 (2015).
[27] M. R. Guassi, G. S. Diniz, N. Sandler, and F. Qu, Phys. Rev. B **92**, 075426 (2015).
[28] M. M. Grujić, M. Z. Tadić, and F. M. Peeters, Phys. Rev. Lett. **113**, 046601 (2014).
[29] D. Midtvedt, C. H. Lewenkopf, and A. Croy, arXiv:1509.02365.
[30] H. Rostami, R. Roldán, E. Cappelluti, R. Asgari, and F. Guinea, Phys. Rev. B **92**, 195402 (2015).
[31] A. Cortijo, Y. Ferreirós, K. Landsteiner, and M. A. H. Vozmediano, Phys. Rev. Lett. **115**, 177202 (2015).
[32] S.-H. Bae, Y. Lee, B. K. Sharma, H.-J. Lee, J.-H. Kim, and J.-H. Ahn, Carbon **51**, 236 (2013).
[33] R. Shimano, G. Yumoto, J. Y. Yoo, R. Matsunaga, S. Tanabe, H. Hibino, T. Morimoto, and H. Aoki, Nat. Commun. **4**, 1841 (2013).
[34] B. Dong, P. Wang, Z.-B. Liu, X.-D. Chen, W.-S. Jiang, W. Xin, F. Xing, and J.-G. Tian, Nanotechnology **25**, 455707 (2014).
[35] M. Oliva-Leyva and G. G. Naumis, Phys. Rev. B **88**, 085430 (2013).
[36] F. M. D. Pellegrino, G. G. N. Angilella, and R. Pucci, Phys. Rev. B **81**, 035411 (2010).
[37] M. Oliva-Leyva and G. G. Naumis, J. Phys.: Condens. Matter **26**, 125302 (2014).
[38] M. Oliva-Leyva and G. G. Naumis, J. Phys.: Condens. Matter **26**, 279501 (2014).
[39] V. M. Pereira, R. M. Ribeiro, N. M. R. Peres, and A. H. Castro Neto, Europhys. Lett. **92**, 67001 (2010).

[40] G.-X. Ni, H.-Z. Yang, W. Ji, S.-J. Baeck, C.-T. Toh, J.-H. Ahn, V. M. Pereira, and B. Özyilmaz, Adv. Mater. **26**, 1081 (2014).
[41] M. Oliva-Leyva and G. G. Naumis, 2D Mater. **2**, 025001 (2015).
[42] L. Tarruell, D. Greif, T. Uehlinger, G. Jotzu, and T. Esslinger, Nature (London) **483**, 302 (2012).
[43] K. K. Gomes, W. Mar, W. Ko, F. Guinea, and H. C. Manoharan, Nature (London) **483**, 306 (2012).
[44] M. Polini, F. Guinea, M. Lewenstein, H. C. Manoharan, and V. Pellegrini, Nat. Nanotechnol. **8**, 625 (2013).
[45] G. Montambaux, F. Piéchon, J.-N. Fuchs, and M. O. Goerbig, Phys. Rev. B **80**, 153412 (2009).
[46] M. Bellec, U. Kuhl, G. Montambaux, and F. Mortessagne, Phys. Rev. Lett. **110**, 033902 (2013).
[47] J. Feilhauer, W. Apel, and L. Schweitzer, Phys. Rev. B **92**, 245424 (2015).
[48] M. O. Goerbig, J.-N. Fuchs, G. Montambaux, and F. Piéchon, Phys. Rev. B **78**, 045415 (2008).
[49] M. I. Katsnelson, *Graphene: Carbon in Two Dimensions* (Cambridge University Press, Cambridge, 2012).
[50] M. Oliva-Leyva and G. G. Naumis, Phys. Lett. A **379**, 2645 (2015).
[51] G. Volovik and M. Zubkov, Ann. Phys. (NY) **340**, 352 (2014).
[52] G. Volovik and M. Zubkov, Ann. Phys. (NY) **356**, 255 (2015).
[53] Y. Hasegawa, R. Konno, H. Nakano, and M. Kohmoto, Phys. Rev. B **74**, 033413 (2006).
[54] K.-i. Sasaki and R. Saito, Prog. Theor. Phys. Suppl. **176**, 253 (2008).
[55] M. A. H. Vozmediano, M. I. Katsnelson, and F. Guinea, Phys. Rep. **496**, 109 (2010).
[56] K. Ziegler, Phys. Rev. Lett. **97**, 266802 (2006).
[57] K. Ziegler, Phys. Rev. B **75**, 233407 (2007).
[58] V. P. Gusynin, S. G. Sharapov, and J. P. Carbotte, Int. J. Mod. Phys. B **21**, 4611 (2007).
[59] T. Stauber, N. M. R. Peres, and A. K. Geim, Phys. Rev. B **78**, 085432 (2008).
[60] R. R. Nair, P. Blake, A. N. Grigorenko, K. S. Novoselov, T. J. Booth, T. Stauber, N. M. R. Peres, and A. K. Geim, Science **320**, 1308 (2008).
[61] S.-M. Lee, S.-M. Kim, M. Na, H. Chang, K.-S. Kim, H. Yu, H.-J. Lee, and J.-H. Kim, Nano Res. **8**, 2082 (2015).